Geomechanics and Engineering, *Vol. 26, No. 3 (2021) 235-251*
https://doi.org/10.12989/gae.2021.26.3.235

Data-driven framework for predicting ground temperature during ground freezing of a silty deposit

Khanh Pham[1,2a], Sangyeong Park[3b], Hangseok Choi[3c] and Jongmuk Won*[4]

[1]*Department of Civil Engineering, International University, Ho Chi Minh City, Vietnam*
[2]*Vietnam National University, Ho Chi Minh City, Vietnam*
[3]*School of Civil, Environmental, & Architectural Engineering, Korea University, Seoul, 02841, Republic of Korea*
[4]*Department of Civil and Environmental Engineering, University of Ulsan, Ulsan, 44610, Republic of Korea*

(Received December 17, 2020, Revised July 2, 2021, Accepted July 22, 2021)

Abstract. Predicting the frozen zone near the freezing pipe in artificial ground freezing (AGF) is critical in estimating the efficiency of the AGF technique. However, the complexity and uncertainty of many factors affecting the ground temperature cause difficulty in developing a reliable physical model for predicting the ground temperature. This study proposed a data-driven framework to accurately predict the ground temperature during the operation of AGF. Random forest (RF) and extreme gradient boosting (XGB) techniques were employed to develop the prediction model using the dataset of a field experiment in the silty deposit. The developed ensemble models showed relatively good performance ($R^2 > 0.96$), yet the XGB model showed higher accuracy than the RF model. In addition, the evaluated mutual information and importance score revealed that the environmental attributes (ambient temperature, surface temperature, humidity, and wind speed) can be critical in predicting ground temperature during the AFG operation. The prediction models presented in this study can be utilized in evaluating freezing efficiency at the range of geotechnical and environmental attributes.

Keywords: artificial ground freezing; data-driven framework; extreme gradient boosting; mutual information; random forest

1. Introduction

In the last century, the increase in traffic load motivated the development of underground infrastructure. Excavation-related construction projects have been encountered unfavorable conditions (e.g., extremely soft ground or high-water pressure) more frequently. Owing to significant advantages of the rapid increase in soil strength, the artificial ground freezing method (AGF) has been emerging as an excellent environmentally-friendly alternative to the cement-based conventional grouting techniques in civil engineering projects such as tunneling (Li *et al.* 2006, Hu *et al.* 2018), excavation (Mandolini and Viggiani 2017), shaft sinking (Schmall and Maishman 2007), and mining (Vitel *et al.* 2016a).

Quantifying the development of frozen zone in the vicinity of refrigerant (or predicting the ground temperature) is critical in the design of the AGF system. Therefore, several experimental studies have been performed to determine the freezing behaviors of the ground (Jones and Brown 1979, Lu *et al.* 2016, Liu *et al.* 2016). The thermal properties of the ground were identified as complex functions of the volume fractions of soil, water and air, soil mineralogy, and ground temperature (Pimentel *et al.* 2012, Andersland and Ladanyi 2013, Russo *et al.* 2015, Hu *et al.* 2018). Thus, pre-assumptions and hypotheses on the freezing characteristic curve, Clapeyron equation, and thermal/hydraulic conductivity relationships are required in the conventional physics-based models for thermal analysis (Kurylyk and Watanabe 2013). Besides, the efficiency of AGF can be affected by the freezing system and ground conditions, as reported in the literature: material of freezing pipe (Cai *et al.* 2020), groundwater condition (Vitel *et al.* 2016a), the configuration of the freezing pipe (Marwan *et al.* 2016), and salinity effect (Rouabhi *et al.* 2018, Wang *et al.* 2018), unfrozen water content (Tang *et al.* 2020), freeze-thaw cycle (Xu *et al.* 2018, Yilmaz and Fidan 2018). In addition, environmental conditions (e.g., wind speed, humidity, and ambient and surface temperatures) can influence the thermal behaviors of the ground, particularly when exposing to the atmosphere. Tai *et al.* (2018) exhibited the effect of sunny-shady slope and strike on the thermal regime of subgrade along the high-speed highway in the cold region.

Fundamentally, the physics-based models for estimating the development of frozen zone in the vicinity of refrigerants (Lee *et al.* 2014, Marwan *et al.* 2016, Vitel *et al.* 2016b, Tounsi *et al.* 2020) have been formulated by coupling the physical phenomena occurring within the ground during the freezing process (e.g., mass transfer, heat transfer, and deformation induced by thermal loads). These models have certain achievements in estimating the

*Corresponding author, Assistant Professor
E-mail: jmwon@ulsan.ac.kr
[a]Lecturer
[b]Graduate Student
[c]Professor

Copyright © 2021 Techno-Press, Ltd.
http://www.techno-press.org/?journal=gae&subpage=7
ISSN: 2005-307X (Print), 2092-6219 (Online)

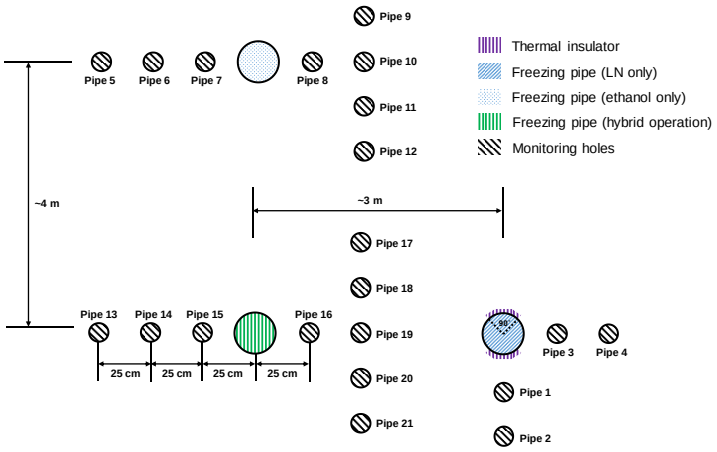

Fig. 1 Layout of freezing pipes and temperature-measuring holes (monitor pipes) at the testbed

response of ground under various freezing conditions. Nevertheless, predicting the frozen zone in AGF is challenging using the abovementioned models owing to the high uncertainty and non-linear effects of various factors involved in the freezing process. For example, the phase change of soils leads to the change in thermal properties (e.g., thermal conductivity, heat capacity), which are a function of many factors including soil mineralogy, porosity, degree of saturation, and salinity. This heterogeneous and stochastic nature of thermal properties may lead to the unreliable prediction of temperature in AGF by physics-based models.

The emergence of machine learning (ML) algorithms provides excellent substitutes for physics-based models in geotechnical engineering (Armaghani *et al.* 2020a, 2020b; Erzin and Cetin 2014; Gao and He 2017). One of the significant advantages of the ML-based models is the ability of learning and recognizing the behavior patterns of the complex system under various conditions. Therefore, their predictions, theoretically, asymptote to the system's nature. For the thermal response of soils, great attention have been drawn to utilize the ML to enhance the operation of geothermal energy systems (Perera *et al.* 2014, Arat and Arslan 2017, Makasis *et al.* 2018). In the field of AGF, only a few studies have been applied ML to model the response of ground to the freezing process (Chen *et al.* 2009, Ren *et al.* 2019). Nevertheless, dealing with a complex database including unpredictable distribution of attributes can downgrade the performance of typical ML models such as neural networks and support vector machines (Géron 2019).

Ensemble learning has been developed to enhance the performance of single learning algorithms. The improvement is based on embracing the diversity of the base predictors, therefore, being capable of learning different perspectives of the database. The techniques have been commonly applied to obtain diverse predictors including bagging, stacking, and boosting. Despite the noticeable advantages of ensemble models in many fields, it has not been applied in AGF modeling to date.

The primary objective of this study is to develop a reliable data-driven framework for predicting ground temperature near the freezing pipe during AGF operation. Random forest (RF) and extreme gradient boosting (XGB) learning methods were employed to predict the temperature variation of the ground during the freezing process. Field experiment data presented in Supplementary Materials were used to formulate the two ensemble models. In addition, mutual information and importance scores were evaluated to identify the potential critical factors affecting the ground temperature. The attributes were categorized into four groups ((1) geotechnical properties; (2) geometry; (3) freezing method; and (4) environmental conditions) in order to assess the impact of geotechnical and environmental attributes on model accuracy.

2. Experimental data

2.1 Field experiment

The database used in this study were obtained from the results of field experiments performed in Ganghwado, South Korea. The testbed was located 0.5 km from the Yellow Sea and primarily composed of a silt deposit. Liquid nitrogen (-196°C) and ethanol (-40°C) were injected into the ground by three injection scenarios: injection of liquid nitrogen for 3 days (open system), circulation of ethanol for about 40 days (closed system), and the injection of liquid nitrogen followed by the circulation of ethanol (hybrid operation, 3-days injection of liquid nitrogen followed by 40 days circulation of ethanol). Three freezing pipes for injecting the refrigerants and twenty-three temperature measuring pipes for the monitoring temperature were installed (Fig. 1).

The freezing pipe with a diameter of 89.1 mm and a length of 5.3 m was designed for the field experiment. The upper 2 m of the freezing pipe was thermally insulated using a 3-cm thick glass wool insulator to induce heat transfer below the groundwater level of the site (2 m). The freezing pipe was composed of an inner (diameter of 21.7 mm) and outer pipe for inducing the heat exchange with the ground while liquid nitrogen or ethanol is transported upward through the outer pipe (the freezing pipe was vertically installed from the surface to 5-m depth). The outlet of the freezing pipe was exposed to the atmosphere for liquid nitrogen (gasified nitrogen is exhausted after heat

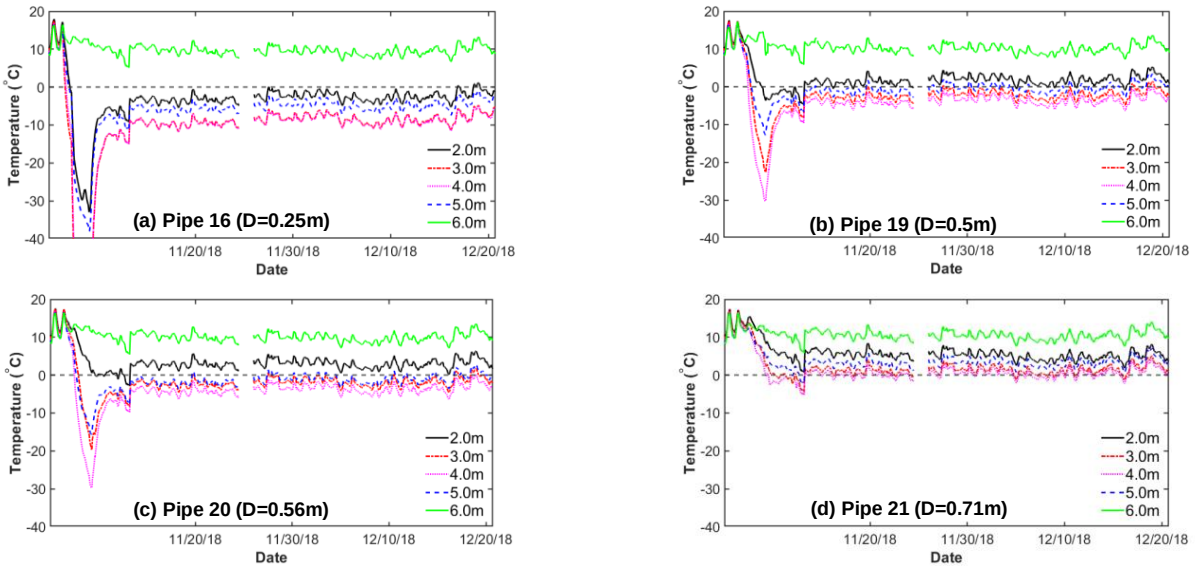

Fig. 2 Monitored temperature at the distance of (a) 0.25 m, (b) 0.5 m, (c) 0.56 m and (d) 0.71 m for the hybrid operation

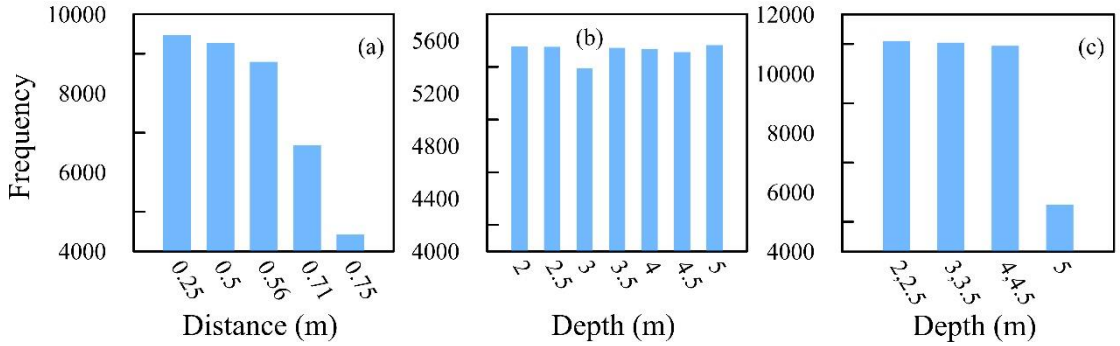

Fig. 3 Histogram of attributes representing the geometry conditions ((a) and (b)) and geotechnical properties (c) Geotechnical properties are summarized in Table 1

Table 1 Geotechnical properties of the dataset at the depth of 2~5 m

Depth (m)	Frequency	Dry density (g/cm^3)	w (%)	LL	PL	λ_{frozen} (W/mK)	$\lambda_{unfrozen}$ (W/mK)
2, 2.5	11105	1.225	42.2	45.1	17.2	2.53	1.13
3, 3.5	11049	1.267	36	33.9	5.7	2.28	1.08
4, 4.5	10936	1.242	41.5	39.8	9.6	2.39	1.21
5	5565	1.253	36.7	31.4	4.2	2.08	1.15

Note: w = water content, LL = liquid limit, PL = plastic limit, λ_{frozen} = thermal conductivity of frozen soil, $\lambda_{unfrozen}$ = thermal conductivity of unfrozen soil

exchange with the ground) and connected to the freezer for ethanol (for circulation).

In each temperature measuring pipe near the freezing pipe, twelve thermocouples every 0.5 m depth from 0.5 ~ 6 m depth were attached for injecting LN only and 10 thermocouples every 0.5 m depth from 1.5 ~ 6 m depth was attached for another two injection scenarios. The observed temperature at monitoring pipes suggested that the dominant heat transfer occurred in the radial direction and the hybrid operation was efficient in maintaining the large frozen mass of soil over a long period. Fig. 2 shows the example of monitored temperature at the distance of 0.25, 0.5, 0.56, and 0.71 from the freezing pipe. A total of 38,655 data were used to develop ensemble models in the following section. All monitored temperature data for three operations (open system, closed system, and hybrid operation) are illustrated in Figs. S3, S4, and S5 in Supplementary Material. Note that the mean and standard deviation of undisturbed ground temperature at the depth of 0.5 ~ 6 m were 12.6°C and 4.1°C respectively.

The geotechnical properties of the testing site presented in Table 1 demonstrate that the soil in all depths can be classified as ML in the unified soil classification system (USCS). The median particle size of the soil sample was ~ 0.04 mm and 100% of particles was less than 75 μm. Because the measured salinity at the groundwater table (2-

Table 2 Statistical description of numeric variables of the database for groups 3 and 4

Groups	Attributes	Mean	Std	Min	Q1	Median	Q3	Max
Freezing method[(c)] (Group 3)	T_{source} (°C)	-29.43	27.06	-174.11	-29.09	-25.92	-22.79	15.21
	Freezing time (days)	20.57	12.61	0.00	9.21	21.33	31.58	43.21
	$T_{monitored}$ (°C)	-0.46	9.38	-84.84	-3.54	0.33	4.14	20.60
Environmental conditions[(d)] (Group 4)	Wind speed (m/s)	1.55	1.08	0.00	0.80	1.40	2.10	6.70
	Humidity (%)	60.60	20.44	17.00	45.00	61.00	78.00	95.00
	$T_{surface}$ (°C)	2.89	5.98	-7.90	-1.10	1.20	7.30	22.30
	$T_{ambient}$ (°C)	3.13	6.20	-13.00	-0.80	2.90	8.20	15.80

Note: T_{source}: the temperature at the freezing pipe; $T_{monitored}$: monitored temperature; $T_{surface}$: surface temperature; $T_{ambient}$: ambient temperature, (c): from Figs. S2, S3, S4, and S5 and (d): from Korea Meteorological Administration

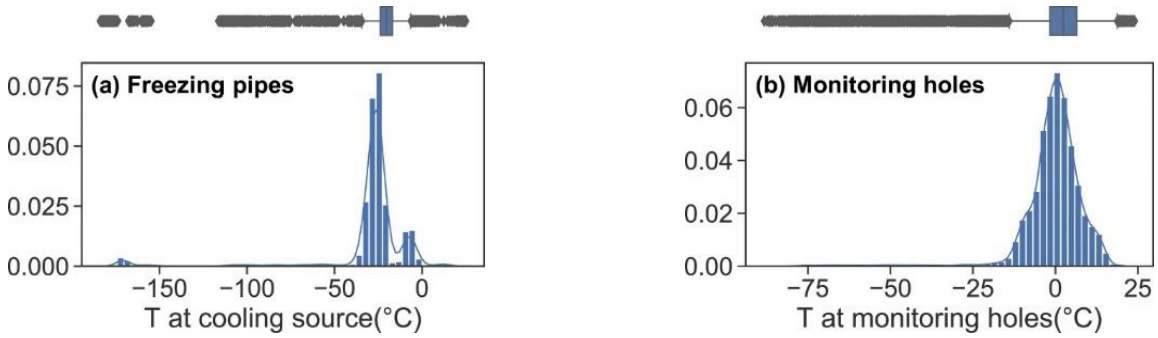

Fig. 4 The probability distribution of temperature dataset in (a) freezing pipes and (b) monitoring holes. The whisker line of box plots here indicates 99.3% coverage for temperature distribution

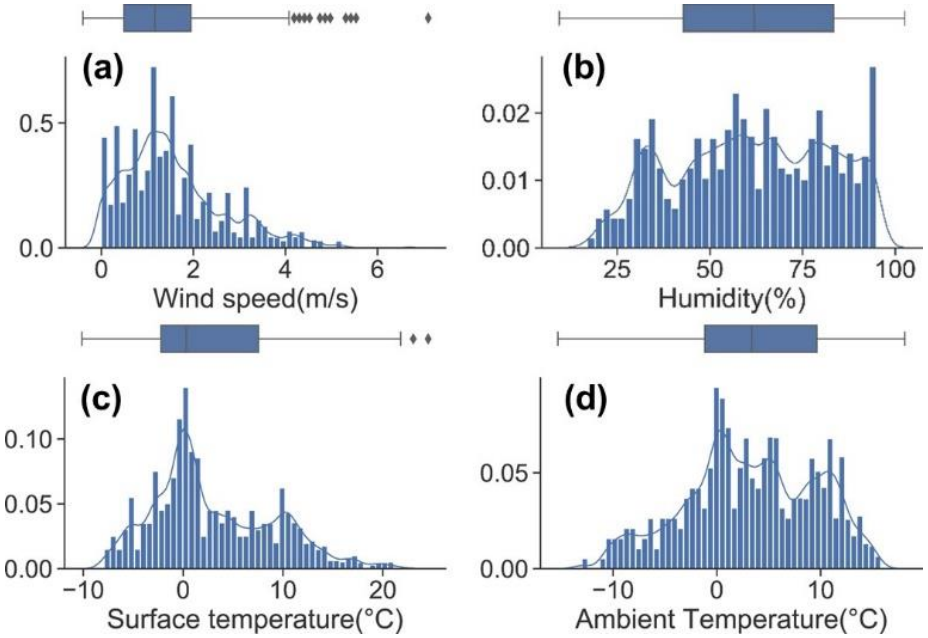

Fig. 5 Distribution of environmental attributes: (a) wind speed, (b) humidity, (c) surface temperature and (d) ambient temperature

m depth) was ~ 0%, the below-zero monitored temperature was regarded as frozen soil.

2.2 Data analysis

The information acquired from the field test was divided into four groups: (1) geotechnical properties, (2) geometry, (3) freezing method, and (4) environmental conditions. Statistically, these attributes fell into two types including categorical variables (i.e., attributes of groups 1 and 2) and numerical variables (i.e., attributes of groups 3 and 4). Fig. 3 presents the histogram of categorical attributes. The imbalance could be observed in the distribution of attributes describing the distance of the monitored points to the

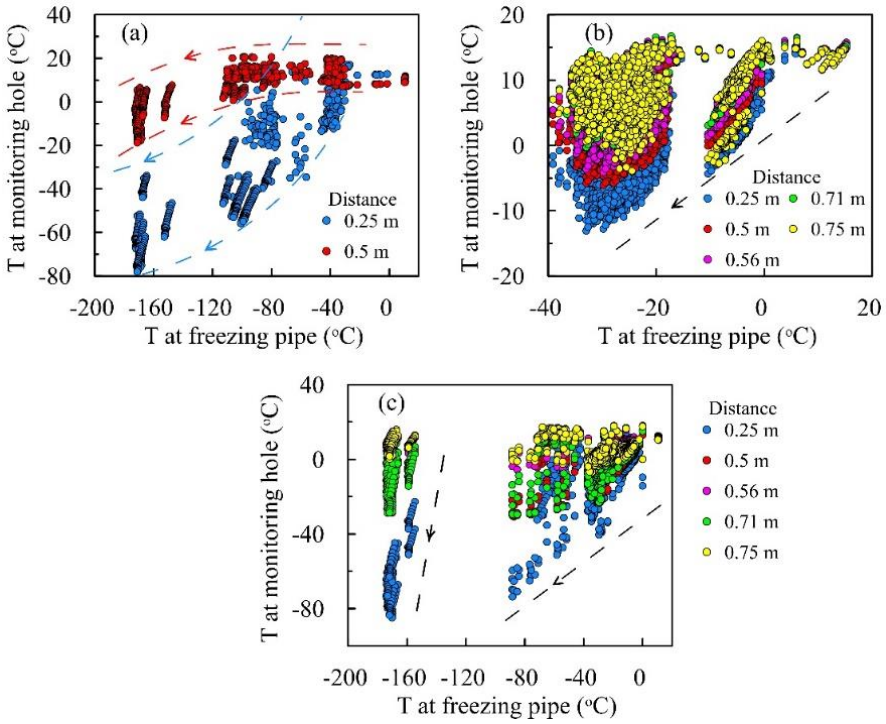

Fig. 6 Correlation between the temperature in the freezing pipe and the monitored holes: (a) open system, (b) closed system, and (c) hybrid operation. Note that the above figures represent temperature data presented in Figs. S3, S4, and S5 as a function of temperature at freezing pipe (Fig S2)

Table 3 Mutual information between the attributes and the temperature at monitoring holes ($T_{monitored}$ in Eq. (1))

No.	Groups	Attributes	Mutual information		
			Closed system	Open system	Hybrid operation
1	Geotechnical properties	Dry density (kN/m^3)	0.952	1.314	0.927
2		Water content (%)	0.952	1.314	0.927
3		LL	0.952	1.314	0.927
4		PL	0.952	1.314	0.927
5		λ_{frozen} (W/mK)	0.952	1.314	0.927
6		$\lambda_{unfrozen}$ (W/mK)	0.952	1.314	0.927
7	Geometry	Depth	1.457	1.891	1.422
8		Distance	1.169	0.682	1.191
9	Freezing method	T_{source} (°C)	6.927	6.334	6.939
10		Freezing time (days)	5.139	3.806	5.165
11	Environmental conditions	Wind speed (m/s)	2.964	3.306	2.969
12		Humidity (%)	3.625	2.801	3.604
13		$T_{surface}$ (°C)	4.261	3.169	4.282
14		$T_{ambient}$ (°C)	4.444	3.49	4.423

freezing pipe (Fig. 3(a)) and the geotechnical attributes (Fig. 3(c)).

Table 2 summary the statistical descriptions of the database. It should be noted that the distributions of numeric attributes in Table 2 are laid on different ranges, which may affect the performance of ML algorithms such as neural networks and support vector machine.

Fig. 4 presents the distribution of temperature in the freezing pipes and monitoring holes. The distribution of temperature in the freezing pipes was in the range from -174.11 to 15.21°C, which was majorly centered from -29.09 to -22.79°C. The distribution of temperature in the monitoring holes ranged from -84.84 to 20.6°C and mostly laid on the range from -3.54 to 4.14°C. According to Tukey's rule, the data monitored in the freezing pipe during injecting liquid nitrogen (LN) were considered as the outliers in these two distributions. Noticeably, the distribution of the monitored temperature likely followed

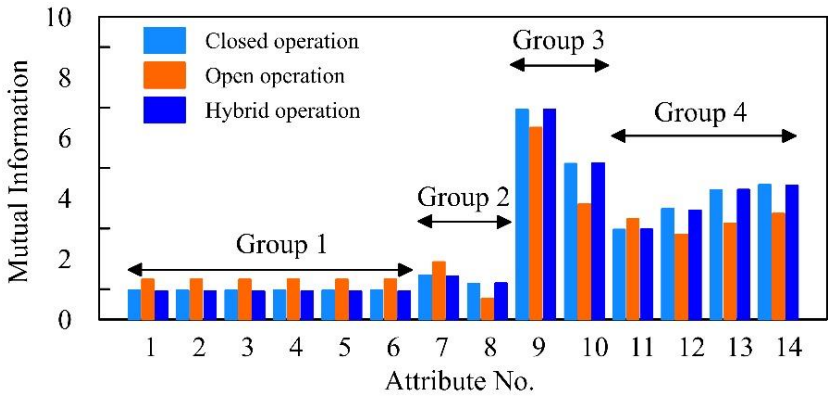

Fig. 7 Illustration of evaluated mutual information between attributes and monitored temperature in Table 3

the Gaussian distribution.

Fig. 5 presents the probability distribution of the environmental attributes during the field experiment. According to the Beaufort scale, the wind was classified as a moderate breeze for only a few days, with wind speed ranging from 5.5 to 7.9 m/s. In contrast, for the entire duration, the wind was categorized as light air to a light breeze, with wind speed ranging from 0.8 to 2.1 m/s. The humidity varied over a relatively broad range from 17 to 100%. The ambient temperature varied from -13 to 15.8°C, mostly being centered in the range from -0.3 to 8.5°C. The surface temperature presented a relatively broader range from -7.9 to 22.3°C. Note that the outliers were detected in the distributions of the wind speed and the surface temperature.

2.3 Relation between attributes and monitored temperature

The temperature in the freezing pipe (T_{source}) is one of the most significant factors governing the development of the frozen zone. Fig. 6 presents the scatter plot for the relationship between the temperature in the freezing pipes and the monitored holes for three injection scenarios (open system, closed system, and hybrid operation).

The apparent correlation between the temperature at the monitoring hole ($T_{monitored}$) and freezing pipe (T_{source}) was observed in three injection scenarios, shown by the arrows in Fig. 6. Notably, two clusters of dataset were observed for hybrid operation (Fig. 6(c)) because of using liquid nitrogen followed by the circulation of ethanol. Obviously, $T_{monitored}$ can be a function of distance from the freezing pipe and T_{source}. In addition, for the distance of 0.25 m, the freezing rate represented by the slope at relatively low T_{source} (< -80 °C) is much higher than the freezing rate at relatively high T_{source} as presented in Fig. 6(a). A similar observation was made for T_{source} lower than -120°C at a distance of 0.5 m. Note that the temperature at the freezing pipe ranged from 0 to -180°C for the open system leads to the low temperature at the monitoring hole (Fig. 6(a)), which implies the rapid formation of frozen soil. In contrast, relatively high temperature for the closed system (Fig. 6(b)) results in high temperature at monitoring hole (T > -15°C), implying the low rate of heat extraction (or formation of frozen soil) caused by the relatively low-temperature gradient.

The attributes showed non-Gaussian distribution restricts the applicability of conventional statistical hypothesis tests (e.g., ANOVA and Chi-squared test). Alternatively, this study applied the mutual information (MI) concept from informatics theory to evaluate the association between the attributes of the database and the variation of $T_{monitored}$. It was assumed that set of attributes, v and $T_{monitored}$, are mutually independent (i.e., their joint distribution is a product of their marginals, $p(v,T_{monitored}) = p(v)p(T_{monitored})$). Subsequently, the Kullback-Leibler (KL) divergence (Kullback and Leibler 1951) can be applied to evaluate the dependence of v and $T_{monitored}$:

$$I(v,T_{monitored}) = -\iint p(v,T_{monitored}) \ln \frac{p(v)\times p(T_{monitored})}{p(v,T_{monitored})} dv dT_{monitored} \quad (1)$$

where I(v, $T_{monitored}$) is the MI between v and $T_{monitored}$. Note that $I \geq 0$ and equality occurs if v and $T_{monitored}$ are mutually independent.

Table 3 and Fig. 7 summarize the MI values for three operations. The evaluation results demonstrated more or less the strong relationship between the attributes of freezing methods and T_{source}. Particularly, T_{source} showed the most significant dependency on $T_{monitored}$, which is consistent with the scatter plot presented in Fig. 6. Furthermore, it is notable that the more substantial dependency of environmental attributes than the geotechnical and geometrical attributes was observed, which have been considered as dominant factors in the physics-based model for heat transfer in soils. The evaluated MI shown in Table 3 implies that the influence of environmental attributes for an open system was less significant than the closed system and the hybrid operation.

3. Ensemble learning models

The ensemble learning models can be classified into two groups: parallel learning and sequential learning. This study employed Random Forest (RF) and Extreme Gradient Boosting (XGB) to represent parallel learning and sequential learning, respectively, to develop the prediction models for estimating the variation of ground temperature in AGF.

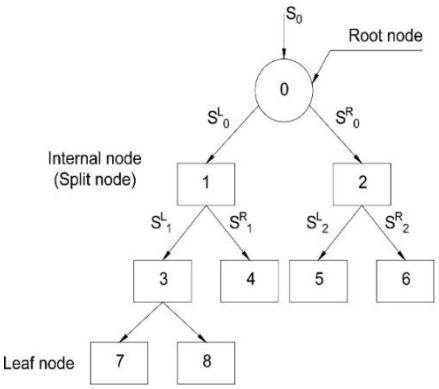

Fig. 8 Typical structure of the decision tree

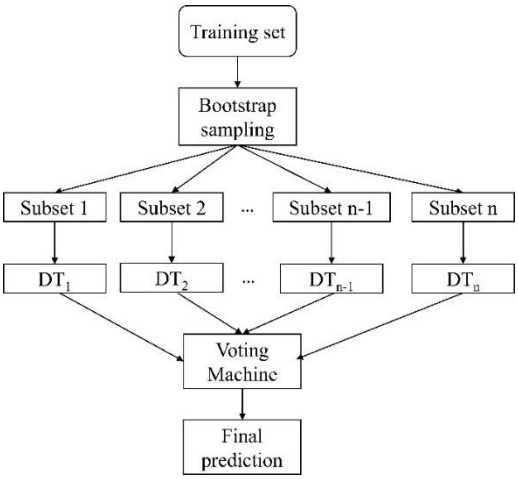

Fig. 9 Flowchart of the random forest algorithm

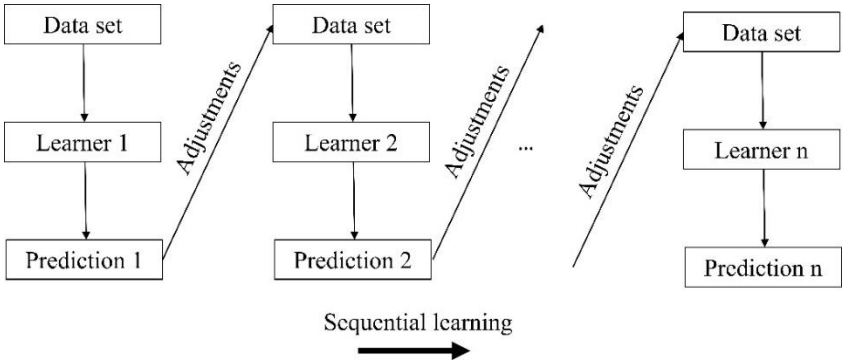

Fig. 10 Flowchart of sequential learning

The above two ensemble models utilize the decision tree (DT) because of its simplified requirements in pre-processing data, reliable performance, and high interpretability. The split function of a DT consists of (i) a filter function to select the features of the input vector; (ii) a parameter to define the approach to separate the data; and (iii) a parameter capturing the threshold of inequality. All these parameters are determined by optimizing the objective function during the training phase. Further details of the DT could be referred to as Shalev-Shwartz and Ben-David (2013). Fig. 8 illustrates the typical structure of DT and the description of RF and XGB is presented in the following sections.

3.1 Random forest algorithm

The advantage of the random forest (RF) algorithm is the ability to use the bagging technique (Breiman 1996) to inject randomness into DTs. Each DT is trained on different subsets during the learning phase with randomly sampling with replacement (bootstrap sampling) from the training set. Following the completion of training, the RF provides the final prediction by averaging the predictions of all the trained DTs. This concept utilizes the diversity in the predictions of the DTs for enhancing the generalization capacity as well as improving the final prediction accuracy. Fig. 9 presents the typical flowchart of RF.

Table 4 Hyperparameters of ensemble learning models

Ensemble model/ Scenario of input features	Scenario I (Full Features)	Scenario II (Omitting geotechnical attributes)	Scenario III (Omitting environmental attributes)
RandomForest	$n_{estimators}$=200; min_samples_split=4; min_samples_leaf=1	$n_{estimators}$=190; min_samples_split=4; min_samples_leaf=1	$n_{estimators}$=200; min_samples_split=2; min_samples_leaf=1
Extreme Gradient Boosting	$n_{estimators}$ =200; max_depth=8; min_child_weight=20; eta=1; subsamples=1	$n_{estimators}$ =200; max_depth=7; min_child_weight=1; eta=1; subsamples=1	$n_{estimators}$ =200; max_depth=10; min_child_weight=8; eta=1; subsamples=1

Note: $n_{estimators}$: number of base predictors; min_samples_split: minimum number of samples required to be split at an internal node; min_samples_leaf: minimum number of samples required to be at the leaf node; max_depth: maximum depth of the tree; min_child_weight: the minimum sum of weights of all samples required in an internal node; eta: learning rate; subsamples: the fraction of samples to be randomly sampled for each DT

Table 5 K-fold cross-validation of the developed ensemble models (k=5)

Scenario No.	RF		XGB	
	RMSE	R^2	RMSE	R^2
I	1.636 ± 0.025	0.969 ± 0.002	1.362 ± 0.02	0.979 ± 0.001
II	1.638 ± 0.028	0.969 ± 0.002	1.361 ± 0.031	0.979 ± 0.001
III	1.806 ± 0.025	0.963 ± 0.002	1.556 ± 0.005	0.972 ± 0.001

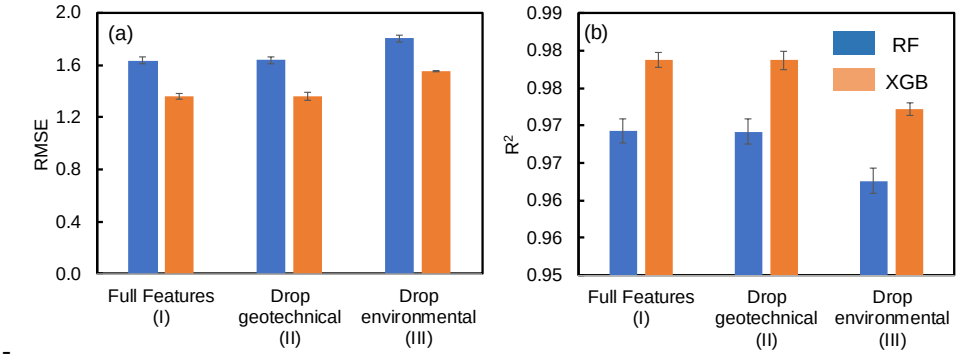

Fig. 11 (a) RMSE and (b) R^2 of RF and XGB models

3.2 Extreme gradient boosting

The boosting method sequentially adds a new base predictor to correct the predecessor. The boosting method can be used for the database with no apparent trend. The noticeable advantage of XGB compared to existing boosting algorithms (AdaBoost and Gradient Boosting) is the ability to support distributed training and integrate with the cloud dataflow system. Also, the XGB provides effective regularized hyperparameters to reduce the risk of overfitting. Fig. 10 presents the learning concepts of sequential learning.

3.3 Model construction

XGB and RF have hyperparameters to regularize the performance. Even though determining these hyperparameters has a critical part of model implementation, manually tuning such hyperparameters is time-consuming. In addition, the state-of-the-art search algorithms (e.g., grid and random search) require covering all the areas of search space. Thus, this study applied Bayesian optimization to determine the optimal set of hyperparameters. During the tuning process, the Bayesian optimization considers the results of the previous steps as prior information to determine the hyperparameters for the next evaluations.

For training the ensemble models, the database (total 38,655 observed temperature data for three operations) was randomly split into the training set and test set with a portion of 80% and 20%, respectively. Because the strong dependency was observed between the environmental attributes and $T_{monitored}$ (Table 3), three scenarios of input features for ensemble models were considered to evaluate the effect of geotechnical or environmental attributes on the prediction accuracy of the models. Table 4 summarizes the hyperparameters of ensemble learning models for each scenario.

4. Results

The performance of two ensemble models (RF and XGB) for predicting ground temperature in AGF was assessed through the evaluated root mean square error (RMSE), coefficient of determination (R^2), and K-fold cross-validation. Note that k = 5 was chosen in this study.

4.1 Prediction of ground temperature

Table 5 and Fig. 11 present the results of the K-fold cross-validation of the developed ensemble models for three

Table 6 R^2 and RMSE values of training and test set for three scenarios

Scenario	R^2				RMSE			
	Train		Test		Train		Test	
	RF	XGB	RF	XGB	RF	XGB	RF	XGB
I	0.992	0.988	0.972	0.981	0.852	1.004	1.600	1.315
II	0.992	0.988	0.971	0.980	0.854	1.015	1.608	1.343
III	0.992	0.987	0.968	0.975	0.848	1.078	1.715	1.511

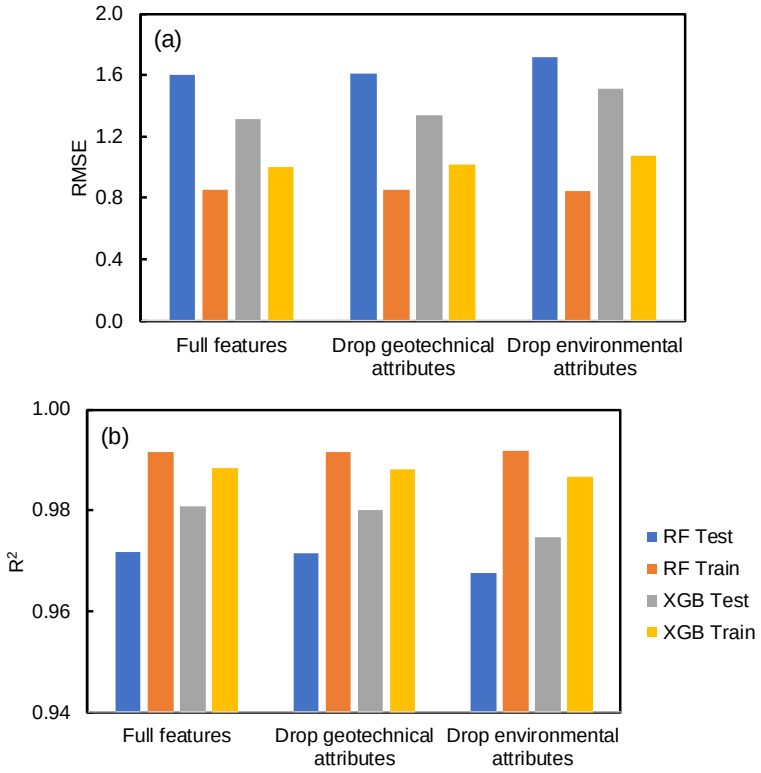

Fig. 12 Illustration of (a) RMSE and (b) R^2 values for training and test set presented in Table 6

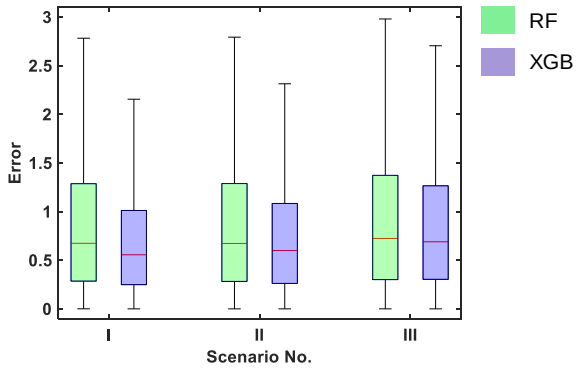

Fig. 13 Error distribution of prediction models on the test set. The edges of the boxes correspond to 25% and 75% coverage, and the red line in the boxes represents the median value of error. The whisker line of each box plot indicates 99 % coverage of error distribution

scenarios presented in Table 4. As shown in Table 5, the XGB framework showed better performance than RF in all prediction models. An average of 16% higher RMSE and 1% higher R^2 was observed when XGB was applied.

It is notable that omitting environmental attributes (scenario No. 3) led to increased RMSE and decreased R^2 for RF and XGB as shown in Fig. 11. In contrast, omitting geotechnical attributes showed comparable values of RMSE and R^2 compared with those values of full feature (scenario No. 1). This implies the significance of environmental

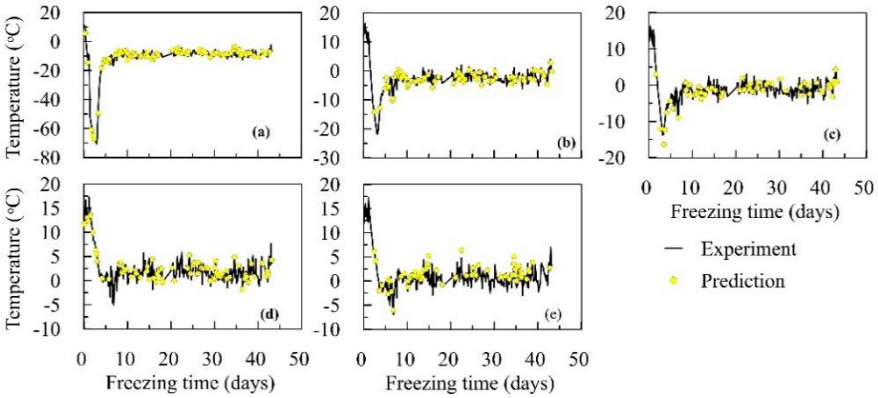

Fig. 14 Prediction of ground temperature for the hybrid operation (LN + ethanol) using XGB model developed in this study (trained with full input feature)

Table 7 Importance scores of attributes for RF and XGB models

Attributes	RF	XGB
Dry density (kN/m^3)	0.001	0.023
Water content (%)	0.001	0
LL	0.004	0
PL	0.004	0
λ_{Frozen} (W/mK)	0.004	0
$\lambda_{Unfrozen}$ (W/mK)	0.001	0.007
Depth	0.016	0.041
Distance	0.279	0.515
$T_{sources}$ (°C)	0.513	0.284
Freezing time (days)	0.146	0.077
Wind speed (m/s)	0.007	0.011
Humidity (%)	0.008	0.012
$T_{surface}$ (°C)	0.009	0.014
$T_{ambient}$ (°C)	0.009	0.016

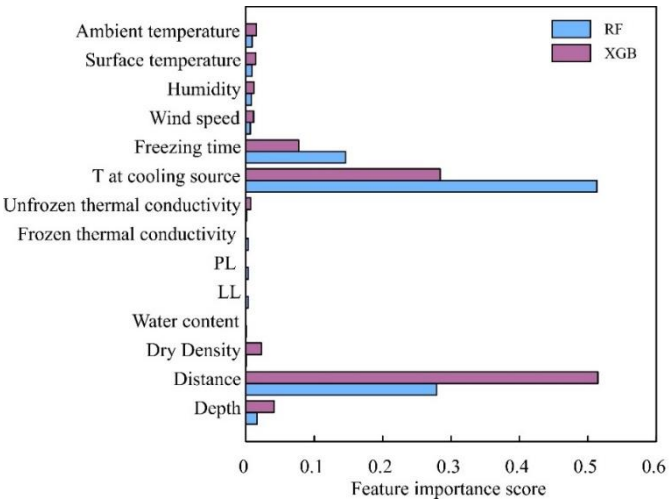

Fig. 15 Illustration of the importance score of attributes presented in Table 7

attributes in predicting the ground temperature in AGF.

Table 6 and Fig. 12 present the RMSE and R^2 values in the training and test for the three scenarios. Again, the XGB model showed better performance than the RF model which is consistent with the result of K-fold cross-validation. In addition, the XGB model trained with full input feature showed the highest prediction accuracy (R^2 = 0.981) as represented by the lowest RMSE value of 1.315. The more

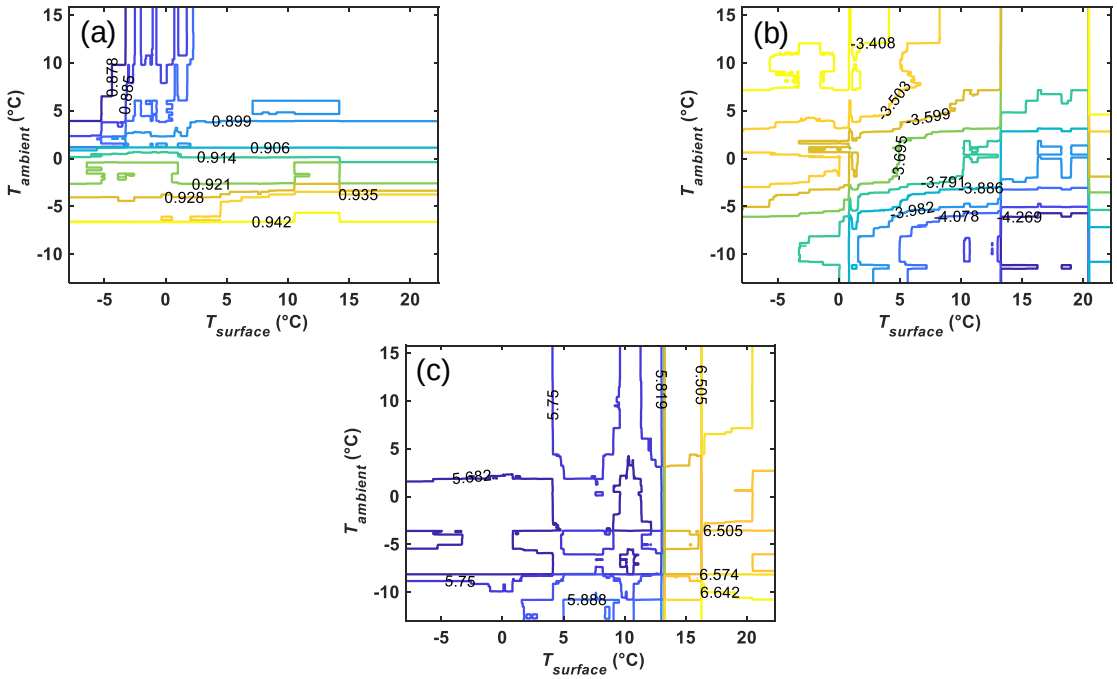

Fig. 16 Contour map of model implementation of hybrid operation at 2 m depth for (a) freezing efficiency, (b) mean temperature of 43 days and (c) standard deviation of temperature. 500 × 500 data were generated using the RF model and the range of $T_{surface}$ and $T_{ambient}$ in Table 1 was adopted here

significant difference in RMSE and R^2 values of training and test for the RF model implies a higher risk of overfitting than the XGB model. The average difference of RMSE and R^2 of training and test set for the RF model were 0.79 and 0.022 whereas those values for the XGB model were 0.35 and 0.009.

The error distribution of RF models in Fig. 13 showed broader ranges than those of XGB models. In addition, the error distribution of XGB models with full input feature showed the narrowest range, which is ranged from 0.25 to 1.01. Fig. 14 illustrates examples of the prediction of ground temperature using the developed XGB model in this study.

4.2 Importance score of attributes

The ensemble models provide the importance score for each input feature according to their impact on the final performance of the models. The importance score was evaluated by the amount that each attribute split point improves the performance measure, weighted by the number of data in the node (sum of importance score is 1). Table 7 and Fig. 15 present the importance scores of attributes for RF and XGB models.

The importance score presented in Table 7 and Fig. 15 demonstrates that the substantial impact of temperature at the cooling source, distance from the refrigerant, and freezing time on the prediction of ground temperature when using developed RF and XGB models. In addition, the higher average importance scores of 0.00825 (RF) and 0.0133 (XGB) for environmental attributes than those of 0.0025 (RF) and 0.005 (XGB) for geotechnical attributes implies the significance of environmental attributes (wind speed, humidity, surface temperature, and ambient temperature) in the prediction of ground temperature in AGF.

4.3 Impact of surface and ambient temperature on freezing efficiency

The freezing efficiency, mean, and standard deviation of ground temperature obtained by the RF model proposed in this study were evaluated. Here, the below-zero temperature was considered as the frozen state of the soil, and the freezing efficiency was quantified as the number of below-zero temperature data divided by the total number of data. Fig. 16 illustrates the surface plots of the freezing efficiency, mean temperature, and standard deviation of hybrid operation obtained by the RF prediction model as a function of $T_{surface}$ and $T_{ambient}$. As seen in Fig. 16, the increase in $T_{surface}$ decreases the freezing efficiency at relatively high $T_{ambient}$ while almost no impact of $T_{surface}$ was evaluated at low $T_{ambient}$. The mean and standard deviation of ground temperature (Fig. 16(b) and 14(c)) implies that an increase in $T_{surface}$ causes the higher fluctuation of ground temperature and an increase in $T_{ambient}$ leads to an increase in ground temperature. The abovementioned findings are more or less intuitive, however, the implementation of the developed prediction models in this study provides the quantitative representation of the impact of given attributes on ground temperature.

5. Discussion

Predicting the frozen zone (i.e., ground temperature) is a

critical part of determining the efficiency of AGF operation. In addition to relatively well known influenced factors affecting the ground temperature in AGF (the temperature at the freezing pipe, distance from the refrigerant, and freezing time), the evaluated mutual information and importance score presented in this study implies the significance of environmental attributes (particularly the surface and ambient temperature) in the prediction of ground temperature. The importance of environmental attributes is consistent with the experimental study presented in Tai *et al.* (2018). Thus, the environmental attributes may be considered for increasing the efficiency of AGF operation.

In the geotechnical aspect, the application of ensemble learning models shown in this study may be limited to silty deposits. The robust model may be developed by using the experimental dataset for other types of soil such as clay or sand. However, the database of field experiments used in this study can be frequently encountered in the practical application of AGF. The geotechnical properties (e.g., dry density, water content, LL, thermal conductivity) are likely relatively constant with time while the environmental attributes significantly change over time during the operation of AGF. Therefore, the framework of developing ensemble learning models in this study can be beneficial in efficiently predicting the ground temperature by taking the high uncertainty of environmental attributes into account. Addressing the uncertainty of environmental attributes in the physics-based model is challenging, therefore, the machine learning-based prediction model can be alternatively used. The high model accuracy of XGB model presented in this study implies the suitability of the XGB technique in predicting ground temperature in AGF.

6. Conclusions

This study presented two ensemble learning models based on random forest (RF) and extreme gradient boosting (XGB) techniques to predict the ground temperature in the artificial ground freezing. The data analysis of experimental data used in this study, evaluated mutual information between attributes and ground temperature, and performance of two developed prediction models conclude:

(i) The experimental data used in this study showed irregular non-Gaussian distribution, which implies the need for a data-driven approach for the prediction of ground temperature.

(ii) The evaluated mutual information between the monitored (ground) temperature and remaining attributes indicates the noticeable impact of environmental attributes on ground temperatures in addition to relatively well-identified attributes such as depth, distance from the freezing pipe, and freezing time. This implies the importance of taking environmental attributes into account for increasing the efficiency of AGF operation.

(iii) A relatively high coefficient of determination and low root mean squared error indicates the reliable performance of RF and XGB models. The XGB model trained with full input features without excluding environmental and geotechnical attributes showed the highest accuracy. The ability to reflect the flexibility of input features and nonlinear characteristics of attributes enable the XGB model to optimize the AGF operation with the consideration of highly uncertain environmental attributes.

Acknowledgments

This work was supported by the National Research Foundation of Korea (NRF) grants (2020R1A6A1A03045059 and 2019R1A2C2086647) funded by the Korea government.

References

Andersland, O.B. and Ladanyi, B. (2013), *An Introduction to Frozen Ground Engineering*, Springer Science & Business Media.

Arat, H. and Arslan, O. (2017), "Optimization of district heating system aided by geothermal heat pump: A novel multistage with multilevel ANN modelling", *Appl. Therm. Eng.*, **111**, 608-623. https://doi.org/10.1016/j.applthermaleng.2016.09.150.

Armaghani, D.J., Mirzaei, F., Shariati, M., Trung, N.T., Shariati, M. and Trnavac, D. (2020a), "Hybrid ANN-based techniques in predicting cohesion of sandy-soil combined with fiber", *Geomech. Eng.*, **20**(3), 191-205. https://doi.org/10.12989/gae.2020.20.3.191.

Armaghani, D.J., Mirzaei, F., Toghroli, A. and Shariati, A. (2020b), "Indirect measure of shear strength parameters of fiber-reinforced sandy soil using laboratory tests and intelligent systems", *Geomech. Eng.*, **22**(5), 397-414. https://doi.org/10.12989/gae.2020.22.5.397.

Breiman, L. (1996), "Bagging predictors", *Mach. Learn.*, **24**(2), 123-140. https://doi.org/10.1007/BF00058655.

Cai, H., Li, P. and Wu, Z. (2020), "Model test of liquid nitrogen freezing-temperature field of improved plastic freezing pipe", *J. Cold Reg. Eng.*, **34**(1), 04020001. https://doi.org/10.1061/(ASCE)CR.1943-5495.0000204.

Chen, Y.L., Azzam, R., Fernandez-Steeger, T.M. and Li, L. (2009), "Studies on construction pre-control of a connection aisle between two neighbouring tunnels in Shanghai by means of 3D FEM, neural networks and fuzzy logic", *Geotech. Geol. Eng.*, **27**(1), 155.-167. https://doi.org/10.1007/s10706-008-9220-5.

Erzin, Y. and Cetin, T. (2014), "The prediction of the critical factor of safety of homogeneous finite slopes subjected to earthquake forces using neural networks and multiple regressions", *Geomech. Eng.*, **6**(1), 1-15. https://doi.org/10.12989/gae.2014.6.1.001.

Gao, W. and He, T.Y. (2017), "Displacement prediction in geotechnical engineering based on evolutionary neural network", *Geomech. Eng.*, **13**(5), 845-860. https://doi.org/10.12989/gae.2017.13.5.845.

Géron, A. (2019), *Hands-On Machine Learning with Scikit-Learn, Keras, and TensorFlow: Concepts, Tools, and Techniques to Build Intelligent Systems*, O'Reilly Media.

Hu, X., Fang, T., Chen, J., Ren, H. and Guo, W. (2018), "A large-scale physical model test on frozen status in freeze-sealing pipe roof method for tunnel construction", *Tunn. Undergr. Sp. Tech.*, **72**, 55-63. http://doi.org/10.1016/j.tust.2017.10.004.

Jones, J.S. and Brown, R.E. (1979), "Design of tunnel support systems using ground freezing", *Eng. Geol.*, **13**(1-4), 375-395. http://doi.org/10.1016/0013-7952(79)90044-9.

Kullback, S. and Leibler, R.A. (1951), "On information and sufficiency", *Ann. Math. Stat.*, **22**(1), 79-86.

Kurylyk, B.L. and Watanabe, K. (2013), "The mathematical representation of freezing and thawing processes in variably-saturated, non-deformable soils", *Adv. Water Resour.*, **60**, 160-177. http://doi.org/10.1016/j.advwatres.2013.07.016.

Lee, D., Choi, H.J., Pham, K., Lee, I.M. and Choi, H. (2014), "Numerical simulation of artificial-freezing propagation for subsea-tunnel construction: Effect of refrigerant temperature and ground water", *Proceedings of the 8th International Symposium on Geotechnical Aspects of Underground Construction in Soft Ground*, Seoul, Korea.

Li, S., Lai, Y., Zhang, M. and Zhang, S. (2006), "Minimum ground pre-freezing time before excavation of Guangzhou subway tunnel", *Cold Reg. Sci. Technol.*, **46**(3), 181-191. http://doi.org/10.1016/j.coldregions.2006.09.001.

Liu, J., Chang, D. and Yu, Q. (2016), "Influence of freeze-thaw cycles on mechanical properties of a silty sand", *Eng. Geol.*, **210**, 23-32. http://doi.org/10.1016/j.enggeo.2016.05.019.

Lu, Y., Liu, S., Weng, L., Wang, L., Li, Z. and Xu, L. (2016), "Fractal analysis of cracking in a clayey soil under freeze-thaw cycles", *Eng. Geol.*, **208**, 93-99. http://doi.org/10.1016/j.enggeo.2016.04.023.

Makasis, N., Narsilio, G.A. and Bidarmaghz, A. (2018), "A machine learning approach to energy pile design", *Comput. Geotech.*, **97**, 189-203. https://doi.org/10.1016/j.compgeo.2018.01.011.

Mandolini, A. and Viggiani, G.M.B. (2017), "Experiences gathered from the construction of Napoli underground", *Procedia Eng.*, **172**, 31-41. http://doi.org/10.1016/j.proeng.2017.02.014.

Marwan, A., Zhou, M.M., Zaki Abdelrehim, M. and Meschke, G. (2016), "Optimization of artificial ground freezing in tunneling in the presence of seepage flow", *Comput. Geotech.*, **75**, 112-125. http://doi.org/10.1016/j.compgeo.2016.01.004.

Perera, K.S., Aung, Z. and Woon, W.L. (2014), "Machine learning techniques for supporting renewable energy generation and integration: A survey BT - data analytics for renewable energy integration", *Proceedings of the International Workshop on Data Analytics for Renewable Energy Integration*, Nancy, France, September.

Pimentel, E., Sres, A. and Anagnostou, G. (2012), "Large-scale laboratory tests on artificial ground freezing under seepage-flow conditions", *Géotechnique*, **62**(3), 227-241. http://doi.org/10.1680/geot.9.P.120.

Ren, J., Vanapalli, S.K., Han, Z., Omenogor, K.O. and Bai, Y. (2019), "The resilient moduli of five Canadian soils under wetting and freeze-thaw conditions and their estimation by using an artificial neural network model", *Cold Reg. Sci. Technol.*, **168**. http://doi.org/10.1016/j.coldregions.2019.102894.

Rouabhi, A., Jahangir, E. and Tounsi, H. (2018), "Modeling heat and mass transfer during ground freezing taking into account the salinity of the saturating fluid", *Int. J. Heat Mass Transf.*, **120**, 523-533. http://doi.org/10.1016/j.ijheatmasstransfer.2017.12.065.

Russo, G., Corbo, A., Cavuoto, F. and Autuori, S. (2015), "Artificial Ground Freezing to excavate a tunnel in sandy soil. Measurements and back analysis", *Tunn. Undergr. Sp. Tech.*, **50**, 226-238. http://doi.org/10.1016/j.tust.2015.07.008.

Schmall, P.C. and Maishman, D. (2007), "Ground freezing a proven technology in mine shaft sinking", Mining Engineering New York Tehn Littleton Colorado, Society for Mining Metallurgy and Exploration, **59**(6).

Shalev-Shwartz, S. and Ben-David, S. (2013), *Understanding Machine Learning: From Theory to Algorithms*, Cambridge University Press.

Tai, B., Liu, J., Yue, Z., Liu, J., Tian, Y. and Wang, T. (2018), "Effect of sunny-shady slopes and strike on thermal regime of subgrade along a high-speed railway in cold regions, China", *Eng. Geol.*, **232**, 182-191. http://doi.org/10.1016/j.enggeo.2017.09.002.

Tang, L., Du, Y., Liu, L., Jin, L., Yang, L. and Li, G. (2020), "Effect mechanism of unfrozen water on the frozen soil-structure interface during the freezing-thawing process", *Geomech. Eng.*, **22**, 245-254. https://doi.org/10.12989/gae.2020.22.3.245.

Tounsi, H., Rouabhi, A. and Jahangir, E. (2020), "Thermo-hydro-mechanical modeling of artificial ground freezing taking into account the salinity of the saturating fluid", *Comput. Geotech.*, **119**, 103382. http://doi.org/10.1016/j.compgeo.2019.103382.

Vitel, M., Rouabhi, A., Tijani, M. and Guérin, F. (2016a), "Modeling heat and mass transfer during ground freezing subjected to high seepage velocities", *Comput. Geotech.*, **73**, 1-15. http://doi.org/10.1016/j.compgeo.2015.11.014.

Vitel, M., Rouabhi, A., Tijani, M. and Guérin, F. (2016b), "Thermo-hydraulic modeling of artificial ground freezing: Application to an underground mine in fractured sandstone", *Comput. Geotech.*, **75**, 80-92. http://doi.org/10.1016/j.compgeo.2016.01.024.

Wang, S., Wang, Q., Qi, J. and Liu, F. (2018), "Experimental study on freezing point of saline soft clay after freeze-thaw cycling", *Geomech. Eng.*, **15**(4), 997-1004. https://doi.org/10.12989/gae.2018.15.4.997.

Xu, J., Wang, Z., Ren, J. and Yuan, J. (2018), "Mechanism of shear strength deterioration of loess during freeze-thaw cycling", *Geomech. Eng.*, **14**(4), 307-314. https://doi.org/10.12989/gae.2018.14.4.307.

Yilmaz, F. and Fidan, D. (2018), "Influence of freeze-thaw on strength of clayey soil stabilized with lime and perlite", *Geomech. Eng.*, **14**(3), 301-306. https://doi.org/10.12989/gae.2018.14.3.301.

GC

Appendix

Table S1 Soil properties at the testbed

Depth (m)	Dry density (γ_d) (g/cm^3)	Water content (w) (%)	Atterberg limits		Thermal conductivity (W/mK)	
			LL (%)	PL (%)	Unfrozen ($\lambda_{unfrozen}$)	frozen (λ_{frozen})
0-0.8	1.219	22.6	42.6	18.5	-	-
1-1.8	1.228	27.4	41.1	14.8	1.09	1.91
2-2.8	1.225	42.2	45.1	17.2	1.13	2.53
3-3.8	1.242	41.5	39.8	9.6	1.21	2.39
4-4.8	1.267	36.0	33.9	5.7	1.08	2.28
5-5.8	1.253	36.7	31.4	4.2	1.15	2.08

Note: λ_{Frozen} was determined at -10°C

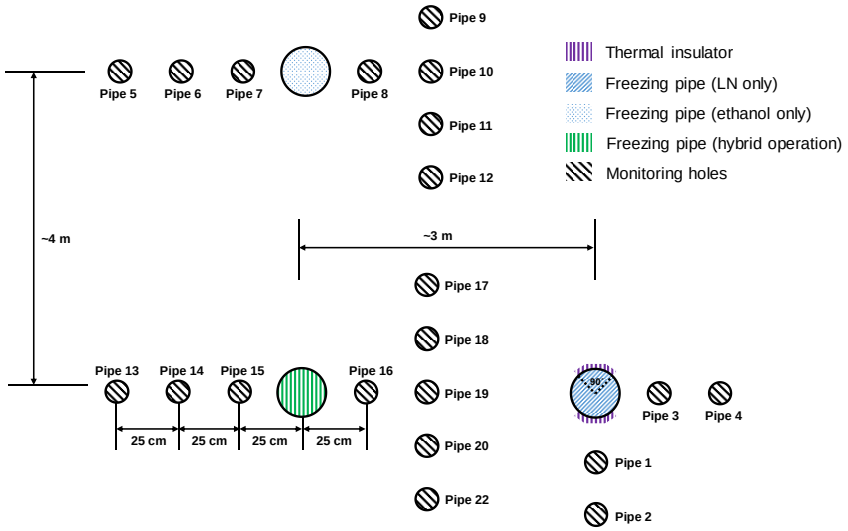

Fig. S1 Layout of freezing pipes and temperature-measuring holes (monitor pipes) at the testbed

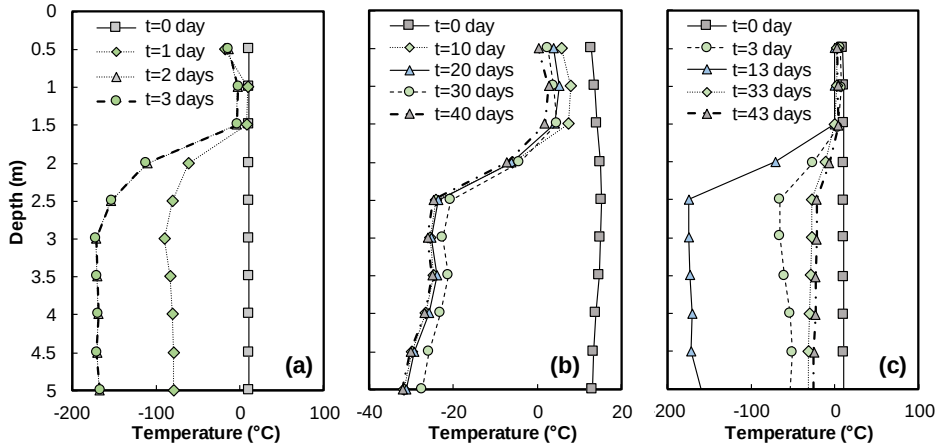

Fig. S2 Temperature profiles of freezing pipes for (a) injecting LN only, (b) circulating ethanol and (c) hybrid operation. The initial ground temperature was approximately 10°C and the legend here represents the date

This Supplementary information briefly presented the testbed conditions and the observed temperature from the experiment. Three methods for freezing were (i) opened system by injecting liquid nitrogen (LN) for 72 hours (3 days), (ii) closed system by circulating ethanol for 40 days, and (iii) hybrid operation by instant freezing of soil with LN and maintaining the frozen soil by circulating ethanol (3 days injection of LN followed by 40 days circulation of ethanol). Note that ethanol was used as a substitution of brine in this experiment.

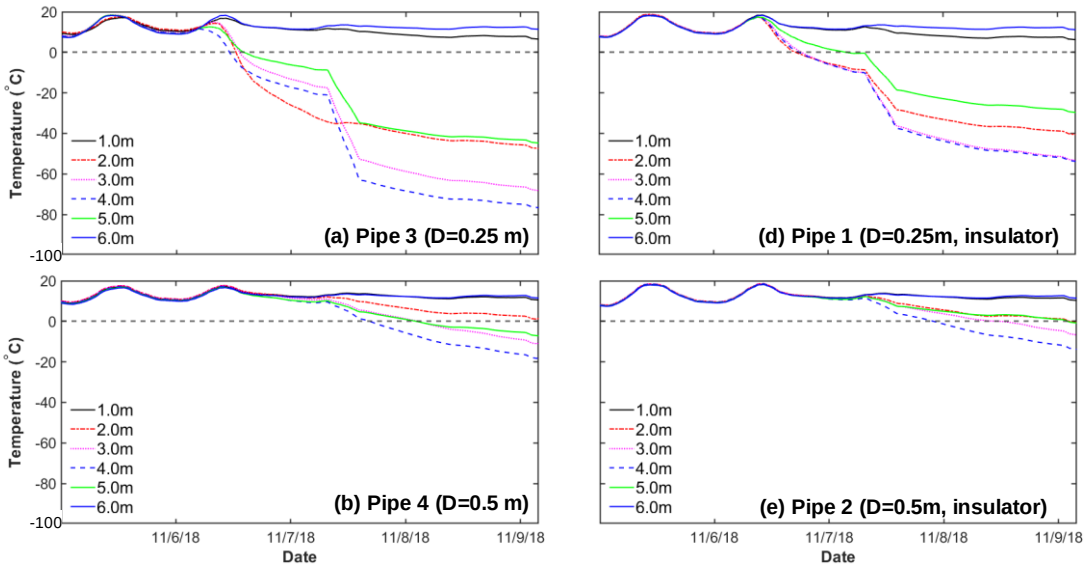

Fig. S3 Profiles of ground temperature obtained from temperature-measuring holes at the depth of 1 - 6 m in the open system (injecting LN only) at the distance (D) of 0.25 and 0.5 m from the freezing pipe (injection period = 3 days)

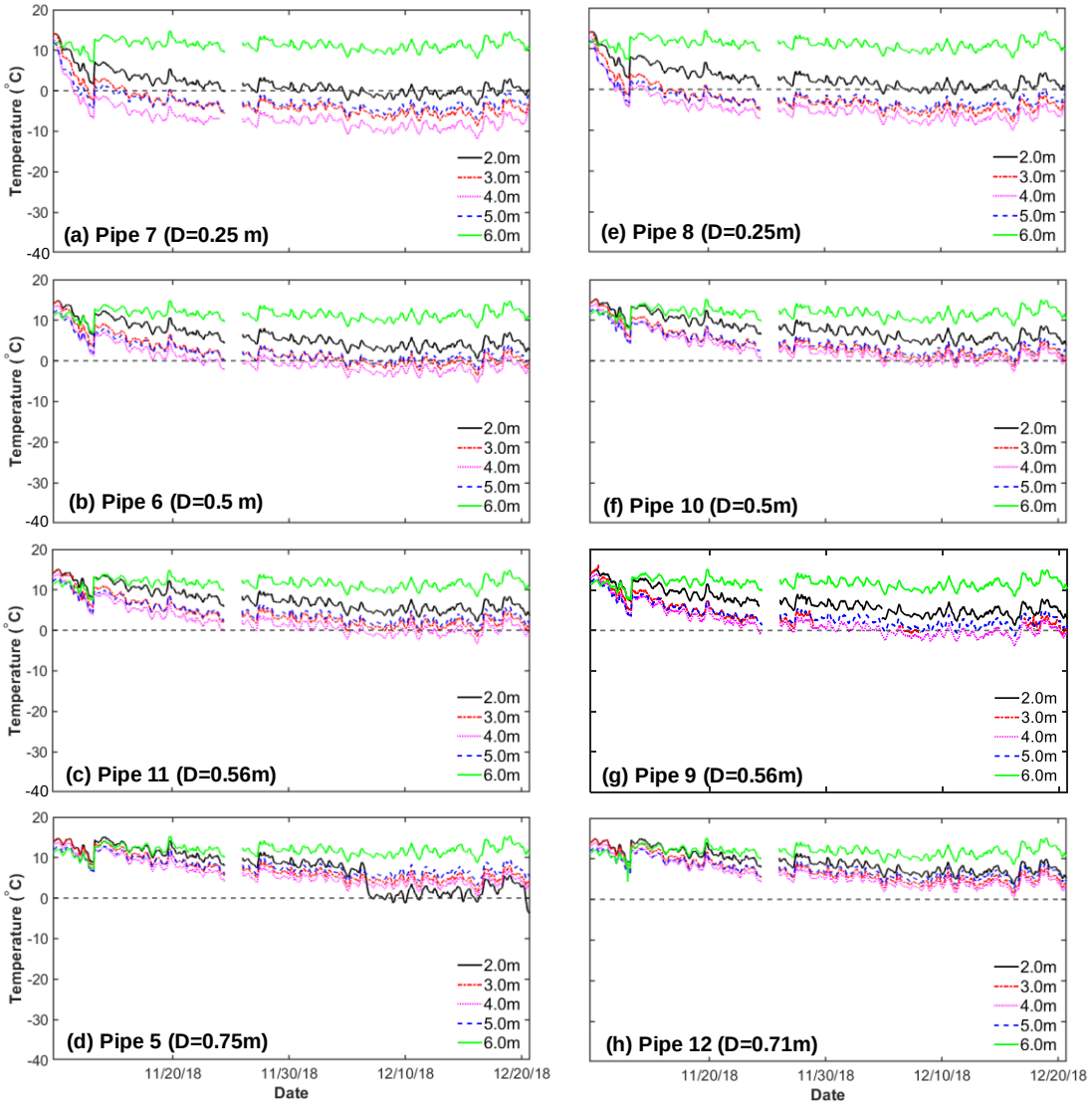

Fig. S4 Profiles of ground temperature obtained from temperature-measuring holes at the depth of 2 - 6 m in a closed system at the distance (D) of 0.25, 0.5, 0.56, 0.71, and 0.75 m from the freezing pipe (injection period = 40 days)

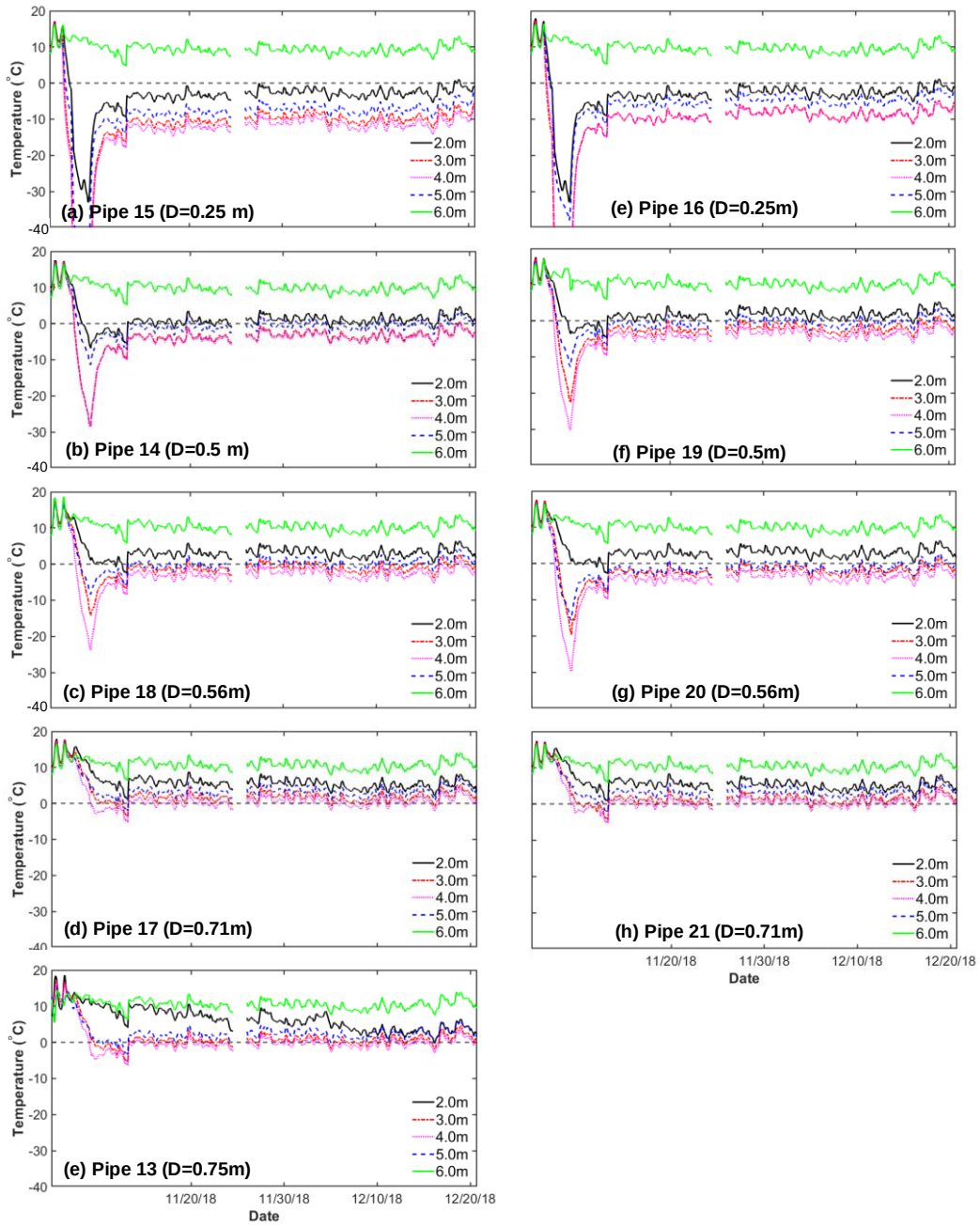

Fig. S5 Profiles of ground temperature obtained from temperature-measuring holes at the depth of 2 - 6 m in the hybrid operation at the distance (D) of 0.25, 0.5, 0.56, 0.71, and 0.75 m from the freezing pipe (injection period = 43 days)

Table S1 and Fig. S1 showed the soil properties at the testbed and layout of the field experiment. The freezing pipes with a length of 5 m were designed to exchange the heat between the refrigerant and the ground. The upper 2 m of the freezing pipes were wrapped in a glass wool insulator to minimize the effect of atmospheric temperature. Furthermore, two insulators with an arc angle of 90° were attached to the freezing pipe for injecting LN only.

The thermal response of the ground to the freezing process was examined from the attached thermocouples at 23 temperature-measuring holes around the freezing pipe as illustrated in Fig. S1. Twelve thermocouples every 0.5 m depth from 0.5 ~ 6 m depth were attached for injecting LN only and 10 thermocouples every 0.5 m depth from 1.5 ~ 6 m depth were attached for another two injection scenarios.

In the case of an opened system, the ground temperature decreased dramatically to approximately -170°C within two days (Fig. S3). In contrast, the closed system required a significant amount of time to achieve a below-zero temperature (Fig. S4). An increase in temperature was observed in the hybrid operation during the injection of ethanol for maintaining the frozen soil (Fig. S5). The similarity in ground temperature profiles at the same distance from the freezing pipe demonstrated the symmetry of heat transfer. Note that the temperature at the direction of attaching insulator is higher than without attaching insulator for injecting LN only (Fig. S3). It should be also noted that the thermocouples at the depth of 1.5 and 2 m of pipe 7

malfunctioned during the freezing process.

For hybrid operation, initial freezing by LN caused an instant decrease in ground temperature. In the period of maintaining the frozen soil by circulating ethanol, the temperature in the freezing pipe was relatively higher than that in the temperature-measuring holes (Fig. S5). Therefore, the direction of heat transfer was from the freezing pipe to the ground in this period, leading to a dramatic increase in ground temperature, particularly at the depth of 3-4 m as shown in Pipe 17 in Fig. S5. Data presented in Figs. S3, S4, and S5 was used to develop the two ensemble models in the manuscript.